Remote Sensing of Environment 152 (2014) 614–626

Contents lists available at ScienceDirect

Remote Sensing of Environment

journal homepage: www.elsevier.com/locate/rse

Global-scale comparison of passive (SMOS) and active (ASCAT) satellite based microwave soil moisture retrievals with soil moisture simulations (MERRA-Land)

A. Al-Yaari [a,b,c], J.-P. Wigneron [a,*], A. Ducharne [b], Y.H. Kerr [d], W. Wagner [e], G. De Lannoy [f], R. Reichle [f], A. Al Bitar [d], W. Dorigo [e], P. Richaume [d], A. Mialon [d]

[a] UMR 1391 ISPA, INRA, F-33140 Villenave d'Ornon, France
[b] UMR 7619 METIS, Université Pierre-et-Marie Curie/CNRS, Paris, France
[c] Geology Department, Faculty of Applied Sciences, Thamar University, Thamar, Yemen
[d] UMR 5126 Centre d'Etudes Spatiales de la BIOsphère (CESBIO) - CNES, CNRS, IRD, Université Toulouse III-, Toulouse, France
[e] Department of Geodesy and Geoinformation, Vienna University of Technology, Vienna, Austria
[f] Global Modeling and Assimilation Office (Code 610.1), NASA Goddard Space Flight Center, Greenbelt, MD 20771, USA

ARTICLE INFO

Article history:
Received 22 April 2014
Received in revised form 15 July 2014
Accepted 16 July 2014
Available online 13 August 2014

Keywords:
SMOS
ASCAT
MERRA-Land
Soil
Moisture
Global
Vegetation
LAI

ABSTRACT

Global surface soil moisture (SSM) datasets are being produced based on active and passive microwave satellite observations and simulations from land surface models (LSM). This study investigates the consistency of two global satellite-based SSM datasets based on microwave remote sensing observations from the passive Soil Moisture and Ocean Salinity (SMOS; SMOSL3 version 2.5) and the active Advanced Scatterometer (ASCAT; version TU-Wien-WARP 5.5) with respect to LSM SSM from the MERRA-Land data product. The relationship between the global-scale SSM products was studied during the 2010–2012 period using (1) a time series statistics (considering both original SSM data and anomalies), (2) a space–time analysis using Hovmöller diagrams, and (3) a triple collocation error model. The SMOSL3 and ASCAT retrievals are consistent with the temporal dynamics of modeled SSM (correlation $R > 0.70$ for original SSM) in the transition zones between wet and dry climates, including the Sahel, the Indian subcontinent, the Great Plains of North America, eastern Australia, and south-eastern Brazil. Over relatively dense vegetation covers, a better consistency with MERRA-Land was obtained with ASCAT than with SMOSL3. However, it was found that ASCAT retrievals exhibit negative correlation versus MERRA-Land in some arid regions (e.g., the Sahara and the Arabian Peninsula). In terms of anomalies, SMOSL3 better captures the short term SSM variability of the reference dataset (MERRA-Land) than ASCAT over regions with limited radio frequency interference (RFI) effects (e.g., North America, South America, and Australia). The seasonal and latitudinal variations of SSM are relatively similar for the three products, although the MERRA-Land SSM values are generally higher and their seasonal amplitude is much lower than for SMOSL3 and ASCAT. Both SMOSL3 and ASCAT have relatively comparable triple collocation errors with similar spatial error patterns: (i) lowest errors in arid regions (e.g., Sahara and Arabian Peninsula), due to the very low natural variability of soil moisture in these areas, and Central America, and (ii) highest errors over most of the vegetated regions (e.g., northern Australia, India, central Asia, and South America). However, the ASCAT SSM product is prone to larger random errors in some regions (e.g., north-western Africa, Iran, and southern South Africa). Vegetation density was found to be a key factor to interpret the consistency with MERRA-Land between the two remotely sensed products (SMOSL3 and ASCAT) which provides complementary information on SSM. This study shows that both SMOS and ASCAT have thus a potential for data fusion into long-term data records.

1. Introduction

Soil moisture is a key variable in land surface and atmospheric systems, and has been identified as one of the "Essential Climate Variables" (System G.C.O., 2010). It plays a fundamental role in the partitioning of precipitation into infiltration and runoff and the partitioning of

* Corresponding author at: UMR 1391 ISPA, INRA, F-33140 Villenave d'Ornon, France. Tel.: +33 557122419; fax: +33 557122420.
E-mail address: wigneron@bordeaux.inra.fr (J.-P. Wigneron).

http://dx.doi.org/10.1016/j.rse.2014.07.013

incoming radiation into sensible and latent heat (Daly & Porporato, 2005; Koster et al., 2004; Western, Grayson, & Blöschl, 2002). Knowledge about global spatial-temporal variability of soil moisture is thus fundamental to improve our understanding of the interactions between the hydrosphere, biosphere, and the atmosphere.

Until now, global-scale studies on this topic were mostly based on modeled data (Seneviratne, Luthi, Litschi, & Schar, 2006; Taylor, de Jeu, Guichard, Harris, & Dorigo, 2012). With the recent advances in global soil moisture retrievals from satellites in the past decade, we are now in the position to study the related processes based on observations. Global surface soil moisture (SSM) datasets have been produced based on active and passive microwave satellite observations, including the Soil Moisture and Ocean Salinity (SMOS) and the Advanced Scatterometer (ASCAT) SSM products (Bartalis et al., 2007; Kerr et al., 2010; Njoku, Jackson, Lakshmi, Chan, & Nghiem, 2003; Owe, de Jeu, & Holmes, 2008). See also Kerr (2007) and Wagner et al. (2007) for a detailed review.

SMOS is the first passive satellite specifically designed to measure SSM (and sea surface salinity) on a global scale (Kerr et al., 2010, 2012). Since its launch in November 2009, SMOS has been recording brightness temperatures at L-Band (1.4 GHz) with an average spatial resolution of 43 km. The SMOS SSM products are derived from the multi-angular and full-polarization brightness temperature observations, using multi-orbital retrieval techniques (Kerr et al., 2012). SMOS SSM is available either in global mode (referred here to as SMOSL3; Jacquette et al., 2010; Kerr et al., 2013) or in swath mode from the European Space Agency (ESA) at the Data Processing Ground Segment (DPGS) (Level 2) (Kerr et al., 2013). In this study, we used the SMOS level 3 (SMOSL3) as its projection (EASE grid) and format (NetCdf) simplified considerably the analysis while retaining all the level 2 characteristics. The ASCAT sensor is a C-band scatterometer (5.2 GHz) operating on-board the Metop since 2006. Wagner, Lemoine, and Rott (1999) proposed a method to retrieve SSM from ERS-1/2 scatterometer backscatter measurements. Naeimi, Scipal, Bartalis, Hasenauer, and Wagner (2009) later improved it and the method is now referred to as the Vienna University of Technology (TU-Wien) change detection algorithm, which is presently employed for ASCAT data.

Since these global SSM observations are relatively new, they have not yet been sufficiently evaluated and their accuracy is still unknown to some degree. It is therefore important (i) to investigate the consistency of the remote sensing products with independent SSM estimates, such as from land surface modeling, and (ii) to characterize their uncertainties. A better knowledge of the skill and uncertainties of the retrievals will help not only to improve the individual products, but also to optimize the fusion schemes adopted to create multi-sensor products, e.g. the essential climate variable (ECV) soil moisture product generated within ESA's Climate Change Initiative (Dorigo et al., 2012; Liu et al., 2011, 2012). This merged product has shown large potential for validating land surface models (Albergel et al., 2013; Loew, Stacke, Dorigo, de Jeu, & Hagemann, 2013) and studying land–atmosphere–biosphere interactions (Barichivich et al., 2014; Miralles et al., 2014).

To date, the validation of the SMOS and ASCAT SSM products has been focused on different regions of the world, primarily by comparing to in situ observations, which are limited in space and time (e.g., Al Bitar et al., 2012; Albergel et al., 2009, 2012; Brocca, Melone, Moramarco, Wagner, & Hasenauer, 2010, Brocca et al., 2011; Leroux, Kerr, Richaume, & Berthelot, 2011; Sanchez, Martinez-Fernandez, Scaini, & Perez-Gutierrez, 2012; Sinclair & Pegram, 2010; Su et al., 2011). A few studies compared microwave based SSM products to model simulations over larger domains (Al-Yaari et al., 2014; Dorigo et al., 2010; Draper et al., 2013; Parrens et al., 2012), thereby improving the knowledge of errors in the satellite data across space and time. At the global scale, there is only, to date, one dedicated SM study that has been conducted to evaluate the SMOS level 2 (SMOSL2) against ASCAT SSM products. Leroux, Kerr, Richaume, and Fieuzal (2013) performed, at the global scale, a comparison between the SMOSL2 SSM products against the Advanced Microwave Scanning Radiometer for EOS (AMSR-E) and ASCAT SSM products taking the European Centre for Medium-Range Weather Forecasts (ECMWF) model simulations as a benchmark for the year 2010. This study showed that SMOS provided best results over Australia, North America, and central Asia in terms of triple collocation errors.

Here, we investigate the consistency of the latest SMOS and ASCAT products, against each other and compared to an independent reference, based on land surface SSM simulations. The analysis is conducted at the global scale, using newly re-processed SSM products, and for the period 05/2010–12/2012. SSM data from the supplemental land surface analysis of the Modern-Era Retrospective analysis for Research and Applications (MERRA-Land) are used as the reference in this study. MERRA-Land data are suitable due to their global availability and their ability to capture the SSM spatial and temporal variability (Reichle et al., 2011). In addition, Albergel et al. (2013) and Yi, Kimball, Jones, Reichle, and McDonald (2011) showed very good performance of MERRA-Land in comparison with other reanalysis products and in situ data.

The objectives of this study are (i) to compare distinct SSM retrieval products derived from satellite-based microwave observations at two different frequency bands, L-band (~1.4 GHz) for the passive SMOSL3 product and C-band (~5 GHz) for the active ASCAT product, (ii) to characterize the global error structure of the SMOSL3 and ASCAT SSM products, and (iii) to understand the spatio-temporal variability of SSM over a variety of biomes and climate regimes at global scale. To achieve these objectives this paper presents (i) a classical time series analysis using a temporal correlation analysis of original SSM and anomalies, unbiased root mean square difference (ubRMSD), and mean bias, (ii) a space–time analysis using Hovmöller diagrams, and (iii) a triple collocation error (TCE) estimation to characterize the spatial distribution of errors in the SMOS and ASCAT retrievals.

The three SSM datasets and the statistical methods used for the evaluation are presented in Section 2, results are presented in Section 3, and discussion and the main conclusions are presented in Section 4.

2. Materials and methods

2.1. Surface soil moisture datasets

Table 1 summarizes the main characteristics of the three SSM datasets (i.e. ASCAT, SMOSL3, and MERRA-Land) considered in this study. ASCAT and SMOSL3 were evaluated with respect to MERRA-Land during the period (05/2010–12/2012).

2.1.1. SMOSL3

The SMOS mission was launched in November 2009 to monitor SSM at a depth of about 3 cm, with an accuracy of at least 0.04 m^3/m^3 at the global scale, and with a 3-day revisit at the equator (Kerr et al., 2001, 2010). SMOS operates at L-band, with ascending overpasses at 06:00 Local Solar Time (LST) and descending overpasses at 18:00 LST (Kerr et al., 2012).

The SMOS level 3 (SMOSL3) SSM products, re-processed global maps of SSM at different temporal resolutions, 1-day, 3-day, 10-day, and monthly, have been recently released by the Centre Aval de Traitement des Données (CATDS; http://catds.ifremer.fr/). The daily SMOSL3 SSM products were used in this study. The main principle of the retrieval algorithm is the same as the one used by ESA for producing the operational level 2 SSM products (Kerr et al., 2012; Wigneron et al., 2007), that is, multi-angular observations are used to simultaneously retrieve SSM (directly quantified in m^3/m^3) and the vegetation optical depth at nadir (τ-NAD) based on a standard iterative minimization approach of a cost function (Wigneron, Waldteufel, Chanzy, Calvet, & Kerr, 2000). SMOSL3 ascending retrievals were selected in this study as they have generally been proven to be more accurate than SMOSL3 descending retrievals (Alyaari et al., 2014; Al-Yaari et al., 2014). The SMOSL3 datasets

Table 1
Main characteristics of the ASCAT, SMOS, and MERRA-Land SSM products.

Soil moisture datasets	Incidence angle (°) of remotely- sensed observations	Data type and frequency	Sampling depth and unit	Temporal coverage	Reference
SMOS level 3 (SMOSL3)	0–55	Remotely sensed (L-band, passive)	~ 0–3 cm (m^3/m^3)	2010–present	Jacquette et al. (2010)
ASCAT	55	Remotely sensed (C-band, active)	~ 0–1 cm (m^3/m^3)	2006–present	Bartalis et al.(2007)
MERRA-Land	–	Reanalysis	0–2 cm (m^3/m^3)	1980–present	Reichle et al.(2011)

provide flags that can be used to screen out questionable SSM retrievals (Jacquette et al., 2010; Kerr, Jacquette, et al., 2013), in particular because of radio-frequency interferences (see Section 2.2 for more details).

It should be noted that, in the present study, we used the latest version available at CATDS. In the near future, new versions of the SMOSL3 products will be produced based on re-processing activities.

2.1.2. ASCAT

ASCAT is a real-aperture radar instrument that operates at C-band (5.255 GHz) on-board the Metop satellite since 2006, which crosses the equator at 21:30 LST for the ascending overpass and at 09:30 LST for the descending overpass.

In this study, we used SSM products generated with the WARP5.5 software provided by TU-Wien, which is the latest version of the algorithm used to produce this SSM dataset. As for SMOSL3, we only considered here morning overpasses, as previous findings indicated that the ascending ASCAT overpass retrievals are less accurate than the descending (i.e., morning) ones (e.g., Brocca et al., 2010).

ASCAT SSM data are provided in terms of degree of saturation, that is, in relative units ranging between 0 (dry) and 100 (saturated). These extremes correspond, respectively, to the lowest and highest values of the observed backscatter over the first few centimeters of soil (<3 cm). As the two other SSM products (SMOSL3 and MERRA-Land) used in this study are expressed in volumetric units, the ASCAT SSM index was converted to volumetric units (m^3/m^3).

Multiplying the degree of saturation by the soil porosity (expressed in m^3/m^3) gives a direct estimate of the volumetric SSM content in m^3/m^3. The value of the soil porosity was estimated from global soil texture and hydraulic soil properties derived, as described by Balsamo et al. (2009), from the Food and Agriculture Organization digital (FAO) soil map (FAO, 2003; Su et al., 2011). The porosity map was provided at a resolution of $5' \times 5'$ and it was interpolated to 25 km, which is consistent with the ASCAT soil moisture resolution. In the ASCAT product, several flags are provided along with the SSM values, including a noise value (ERR) quantifying the uncertainty associated with the retrieved SSM value and a flag associated with the wetland fraction or to the topographic complexity. Readers are directed to Wagner et al. (1999) and Naeimi et al. (2009) for more details on the TU-Wien algorithm and to Wagner et al. (2013) for a full review on the ASCAT SSM Product.

2.1.3. MERRA-Land

The Modern-Era Retrospective analysis for Research and Applications (MERRA) is a global atmospheric reanalysis data product that integrates information from a broad variety of in situ and remote sensing observations of the atmosphere (Rienecker et al., 2011). MERRA-Land is a supplemental data product of land surface hydrological fields (Reichle et al., 2011). The MERRA-Land product is a land-only, off-line, replay of a revised version of the MERRA land model component that benefits from (i) corrections to the precipitation forcing based on merging a gauge-based data product from the NOAA Climate Prediction Centre with MERRA precipitation and (ii) updated parameter values in the rainfall interception model. These changes correct known limitations in the MERRA surface meteorological forcing and yield improved estimates of land surface conditions (Reichle, 2012; Reichle et al., 2011). MERRA-Land SSM is associated with the 0–2 cm (topmost) soil layer and is available hourly at a spatial resolution of 2/3° longitude by 1/2° latitude. The MERRA-land SSM simulations at 6 am and 9 am were averaged and considered as a reference for both SMOS and ASCAT. We used the gridded SSM product expressed in volumetric units (m^3/m^3).

2.2. Pre-processing

Prior to the evaluation, SMOSL3 and ASCAT were filtered based on associated quality flags. Several values are associated with the ASCAT SSM retrievals, as described by (Naeimi et al., 2009): a noise error (ERR), which is based on Gaussian error propagation and which is related to the sensor characteristics and incidence angle uncertainty, an estimated standard deviation of the backscatter signal, etc. The ASCAT data were screened out to remove observations with a noise error (ERR) greater than 14% (Draper, Reichle, De Lannoy, & Liu, 2012). The SMOSL3 product provides a Data Quality indeX (DQX) and a probability of radio frequency interference (RFI). The DQX values, which are provided in volumetric SSM units, quantify the error in the SSM retrieval and the brightness temperature measurement accuracy. RFI originates, for example, from satellite transmissions, aircraft communications, radar, or TV radio-links and contaminates the passive microwave emissions from Earth (Njoku, Ashcroft, Chan, & Li, 2005; Oliva et al., 2012). Fig. 1 shows the global spatial pattern of the probability of RFI occurrence in the SMOS observations, presented as average of the probability of RFI occurrences during the period (2010–2012). In the present study, RFI effects were filtered out, using RFI flags provided in the SMOSL3 product. SMOSL3 SSM values were excluded if one of the following conditions was fulfilled (i) DQX > 0.06, (ii) DQX is equal to fill value, or (iii) percentage of radio frequency interference (RFI_Per) > 30%.

ASCAT, SMOSL3, and the reference MERRA-Land dataset are distributed on different grids and formats. In this study, a nearest neighbor approach (e.g., Draper, Mahfouf, Calvet, Martin, & Wagner, 2011; Rüdiger et al., 2009) was used to re-project all the datasets onto a regular $0.25° \times 0.25°$ grid. Finally, all the three SSM datasets were screened, applying additional static masks, to remove grid cells with (i) steep mountainous terrain, based on a topographic complexity flag (provided with the ASCAT data) greater than 10% (Draper et al., 2012), (ii) open water, identified as having a wetland fraction (provided with the ASCAT data) greater than 5%, and (iii) frozen soil conditions, identified as having soil temperatures (top layer) below 276 K, obtained from MERRA-Land.

It should be noted that all the statistical indicators were computed only when all the three SSM data were available from the different datasets and therefore the number of ASCAT and SMOSL3 SSM data used in the time series are identical, which is illustrated in Fig. 2.

2.3. Comparison using classical metrics

Three classical metrics were calculated between pairs of the remotely sensed (SSM_{RS}) and reference SSM products(SSM_{REF}): (i) Pearson

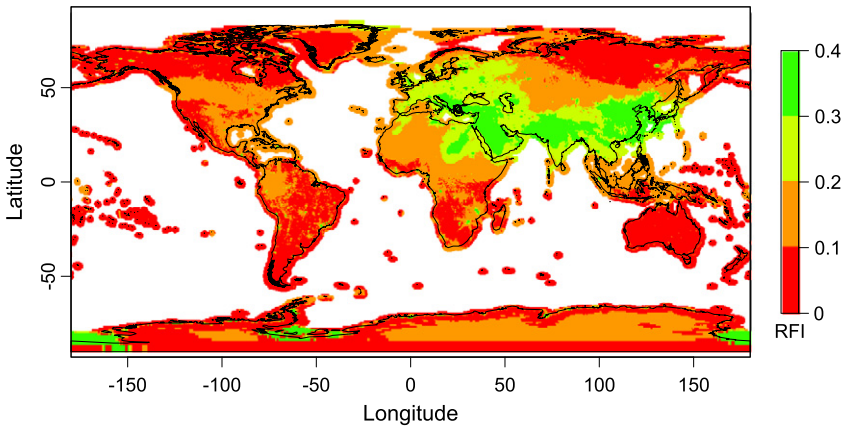

Fig. 1. Three year average (2010–2012) of probability of radio frequency interference occurrences in the SMOS observations.

correlation coefficient (R), (ii) bias, and (iii) unbiased root mean squared difference (ubRMSD). The equations for the calculation of the three indicators are given as follows (Albergel et al., 2012; Brocca et al., 2011; CECR, 2012):

$$R = \frac{\sum_{i=1}^{n}\left(\mathrm{SSM}_{\mathrm{REF}(i)} - \overline{\mathrm{SSM}_{\mathrm{REF}}}\right)\left(\mathrm{SSM}_{\mathrm{RS}(i)} - \overline{\mathrm{SSM}_{\mathrm{RS}}}\right)}{\sqrt{\sum_{i=1}^{n}\left(\mathrm{SSM}_{\mathrm{REF}(i)} - \overline{\mathrm{SSM}_{\mathrm{REF}}}\right)^2 \sum_{i=1}^{n}\left(\mathrm{SSM}_{\mathrm{RS}(i)} - \overline{\mathrm{SSM}_{\mathrm{RS}}}\right)^2}} \quad (1)$$

$$\mathrm{Bias} = \overline{\left(\mathrm{SSM}_{\mathrm{RS}} - \mathrm{SSM}_{\mathrm{REF}}\right)} \quad (2)$$

$$\mathrm{RMSD} = \sqrt{\overline{\left(\mathrm{SSM}_{\mathrm{RS}} - \mathrm{SSM}_{\mathrm{REF}}\right)^2}} \quad (3)$$

$$\mathrm{ubRMSD} = \sqrt{\mathrm{RMSD}^2 - \mathrm{Bias}^2} \quad (4)$$

where n is the number of SSM data pairs, the overbar represents the mean operator, $\mathrm{SSM}_{\mathrm{REF}}$ is the reference SSM (MERRA-Land), and $\mathrm{SSM}_{\mathrm{RS}}$is the satellite-based SSM product (SMOSL3 or ASCAT). We use the term ubRMSD rather than ubRMSE (root mean squared error) since the MERRA-Land SSM values also contain errors and cannot be considered as the "true" SSM values (Entekhabi et al., 2010).

All the above statistical indicators were computed for the original SSM values, expressed in volumetric units (m^3/m^3), and for SSM monthly anomalies for the correlation indicators only. The anomaly time-series are designed to assess the impact of seasonal effects that can unrealistically increase the degree of correlation between two time series (Scipal, Drusch, & Wagner, 2008) and to explore the ability of the ASCAT/SMOSL3 SSM products to capture the short-term variability in the SSM time series. Following Albergel et al. (2009), the anomalies $\mathrm{SSM}_{\mathrm{anom}}(t)$ were calculated as the difference from the mean for a sliding window of 5 weeks, the difference was further scaled to the standard deviation:

$$\mathrm{SSM}_{\mathrm{anom}}(t) = \frac{\mathrm{SSM}_{\mathrm{or}}(t) - \overline{\mathrm{SSM}_{\mathrm{or}}(t-17\ :\ t+17)}}{\sigma[\mathrm{SSM}_{\mathrm{or}}(t-17 : t+17)]} \quad (5)$$

where the overbar and σ symbols denote the temporal mean and standard deviation operators, respectively, $\mathrm{SSM}_{\mathrm{or}}(t)$is the original remotely sensed/reference SSM value at time t; for a sliding window of 5 weeks corresponding to the time interval [t − 17 days, t + 17 days].

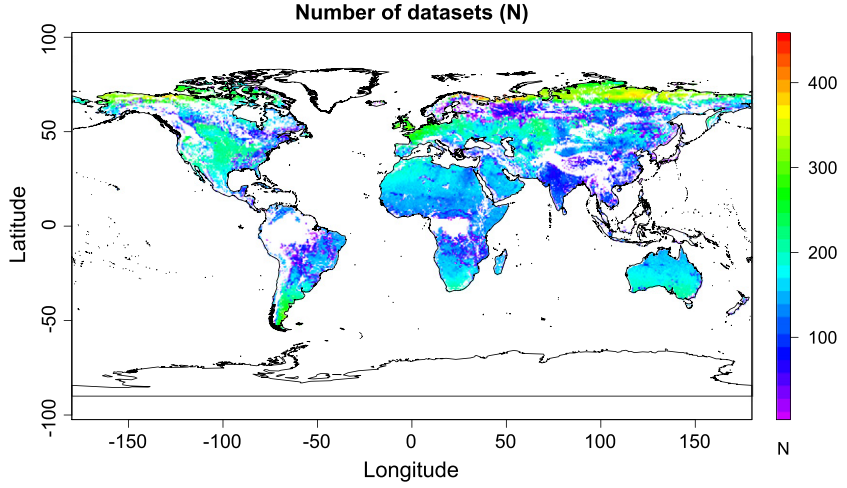

Fig. 2. Number of data used to compare the SMOSL3 and ASCAT datasets.

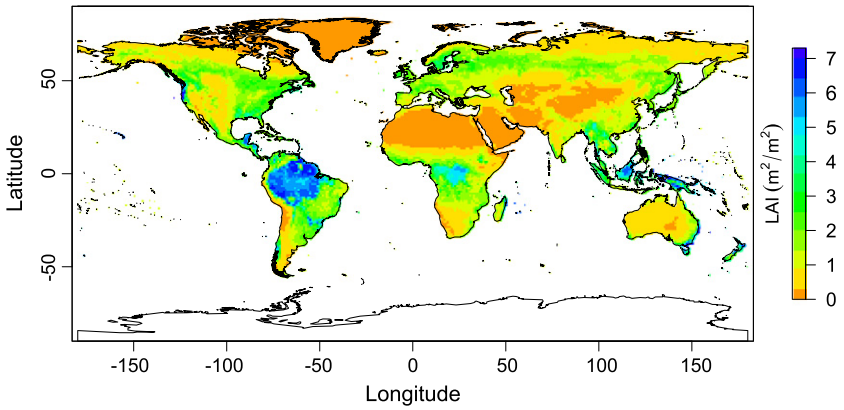

Fig. 3. Global distribution of the long term mean leaf area index (LAI) (Dirmeyer et al., 2006).

Global maps of *R* (original and monthly anomaly), ubRMSD, and bias were calculated for all common pixels on a daily basis between the reference and the SMOSL3 and ASCAT SSM time series. To investigate the effects of the vegetation and to simplify the interpretation of the correlation maps (original and anomalies), the metrics were also averaged according to the long-term mean leaf area index (LAI) values obtained from the Global Soil Wetness Project (Dirmeyer et al., 2006), displayed in Fig. 3.

2.4. Comparison using Hovmöller diagrams (space–time distribution)

A Hovmöller diagram (HD) is a two-dimensional plot that shows the time–latitude variations of a longitudinally averaged variable (Hovmöller, 1949). Here, we used the HD method to compare the spatio-temporal patterns of SSM for SMOS, ASCAT and MERRA-Land at the global scale. The diagrams helped us to investigate the consistency and differences between the three SSM products.

2.5. Comparison using triple collocation error model

The triple collocation error model (TCE) is a powerful statistical tool to estimate the RMSD of a set of at least three linearly related data sources with uncorrelated errors. Stoffelen (1998) introduced the TCE model to evaluate wind vector datasets derived from a model, buoy measurements and scatterometer observations. Scipal, Holmes, de Jeu, Naeimi, and Wagner (2008) later used the TCE to evaluate SSM datasets derived from models and satellites. Then, other authors (e.g., Dorigo et al., 2010; Draper et al., 2013; Loew & Schlenz, 2011; Miralles, Crow, & Cosh, 2010; Parinussa et al., 2011) also used the TCE method to characterize the errors of SSM derived from models and remote sensing.

In this study, TCE was applied to the ASCAT, SMOS, and MERRA-Land SSM products, and specifically to their long-term anomalies, using 2010–2012 time series centered on its mean. The estimated SSM anomalies at time t from product i (denoted $\theta_i(t)$ in the following) are linked to the unknown true SSM $\theta(t)$ by a multiplicative bias term β_i together with an error ε_i:

$$\theta_1(t) = \beta_1.\theta(t) + \varepsilon_1 \tag{6}$$

$$\theta_2(t) = \beta_2.\theta(t) + \varepsilon_2 \tag{7}$$

$$\theta_3(t) = \beta_3.\theta(t) + \varepsilon_3 \tag{8}$$

Note that since centered time series (anomaly from Eq. (5) without normalization) are used here, a constant bias term is not needed in Eqs. (6)–(8). One of the datasets has to be defined as the reference dataset, namely MERRA-Land in this study, with $\beta_1 = 1$. The other two datasets can then be calibrated using $\theta_i^* = \theta_i/\beta_i$ and $\varepsilon_i^* = \varepsilon_i/\beta_i$ in Eqs. (6)–(8) to obtain:

$$\theta_1{}^* = \theta + \varepsilon_1{}^* \tag{9}$$

$$\theta_2{}^* = \theta + \varepsilon_2{}^* \tag{10}$$

$$\theta_3{}^* = \theta + \varepsilon_3{}^* \tag{11}$$

where $\theta_2^*$and θ_3^* are the rescaled measurements, and $\varepsilon_2^*$and ε_3^* are the rescaled random errors (see, e.g., Draper et al., 2013). By pairwise subtraction of Eqs. (9)–(11) and subsequent averaging over the cross-multiplied differences, we obtain:

$$\varepsilon_1{}^{2*} = <(\theta_1{}^* - \theta_2{}^*)(\theta_1{}^* - \theta_3{}^*)> \tag{12}$$

$$\varepsilon_2{}^{2*} = <(\theta_1{}^* - \theta_2{}^*)(\theta_2{}^* - \theta_3{}^*)> \tag{13}$$

$$\varepsilon_3{}^{2*} = <(\theta_1{}^* - \theta_3{}^*)(\theta_2{}^* - \theta_3{}^*)> \tag{14}$$

where $<>$ is the long-term mean, and the square root of the estimated $\varepsilon_i{}^{2*}$ are the triple collocation errors estimates.

The above derivation, and hence the validity of the TCE analysis, is based on the assumptions that the errors ε_i of the three datasets are uncorrelated, and that the three datasets can be linearly modeled as in Eqs. (6)–(8) (Dorigo et al., 2010; Janssen, Abdalla, Hersbach, & Bidlot, 2007; Scipal, Dorigo, & de Jeu, 2010). Because the three datasets are largely independent, TCE can be expected to perform well, but any residual error cross-correlations among the datasets would result in biased error estimates (Yilmaz & Crow, 2012). Finally, to obtain statistically reliable results we restricted our analysis to grid cells where at least 100 observations were available from each dataset.

3. Results

3.1. Spatial Analysis of SSM retrievals at the global scale

Fig. 4 shows global maps of the time series correlation coefficient *R* for original SSM values and monthly anomalies (with only significant correlations, i.e., $p < 0.05$), the ubRMSD, and the bias (Section 2.3). In these maps, SMOSL3 (right panels) and ASCAT (left panels) were

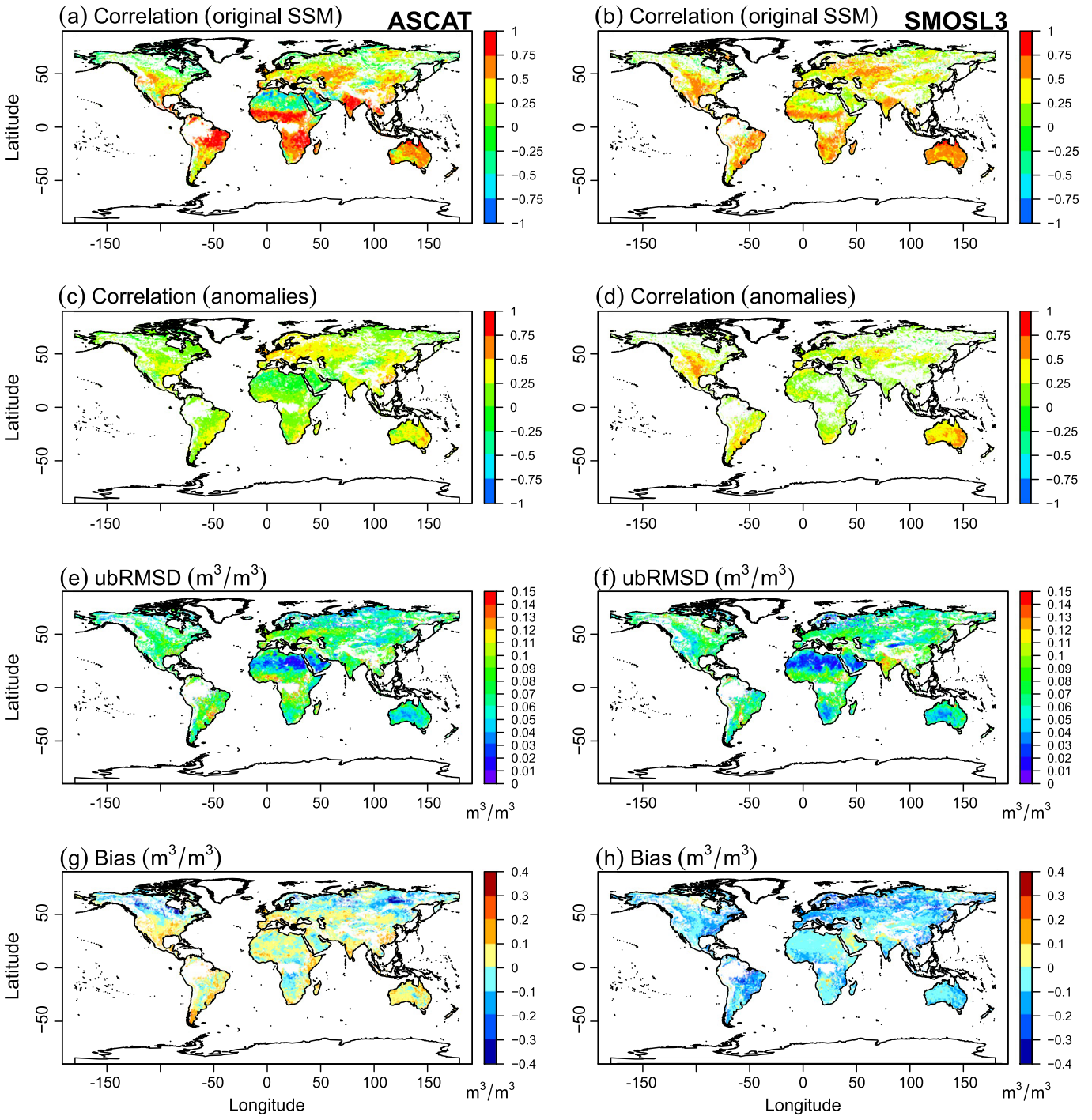

Fig. 4. Pairwise comparison between the SMOSL3 (right panel) and the ASCAT (left panel) SSM datasets with respect to the reference MERRA-Land product in terms of the correlation coefficient (R) based on original SSM data (a and b), on SSM monthly anomalies (c and d), ubRMSD (m^3/m^3; e and f), and bias (m^3/m^3; g and h) during the 05/2010–12/2012 period. Only significant correlations ($p < 0.05$) were plotted.

evaluated against the MERRA-Land reference dataset at each pixel over the 05/2010–12/2012 period.

In general, the metrics for SMOSL3 and ASCAT show a similar spatial correspondence with the MERRA-Land SSM over most of the globe. Fig. 4a and b shows that strong correlations (R is generally greater than ~0.5) between the global remotely sensed and the reference SSM products are found in the transition zones between wet and dry climates (e.g., Sahel), in the Great Plains (USA), western Europe, Australia, India, Kazakhstan, and south-eastern Brazil. This can be explained by the strong seasonal annual cycle of SSM in these regions (Koster et al., 2004).

Conversely, remotely sensed datasets exhibited weak correlations (R is generally less than 0.15) against the reference in arid regions due to the small range of natural variation in the SSM values. The correlations can even be negative between the ASCAT and MERRA-Land data pairs in some arid sites (e.g., Saudi Arabia and North Africa; Fig. 4a). Low correlations for both SMOSL3 and ASCAT in high latitude regions can also be seen in Fig. 4a and b, where the R values drop below 0.20.

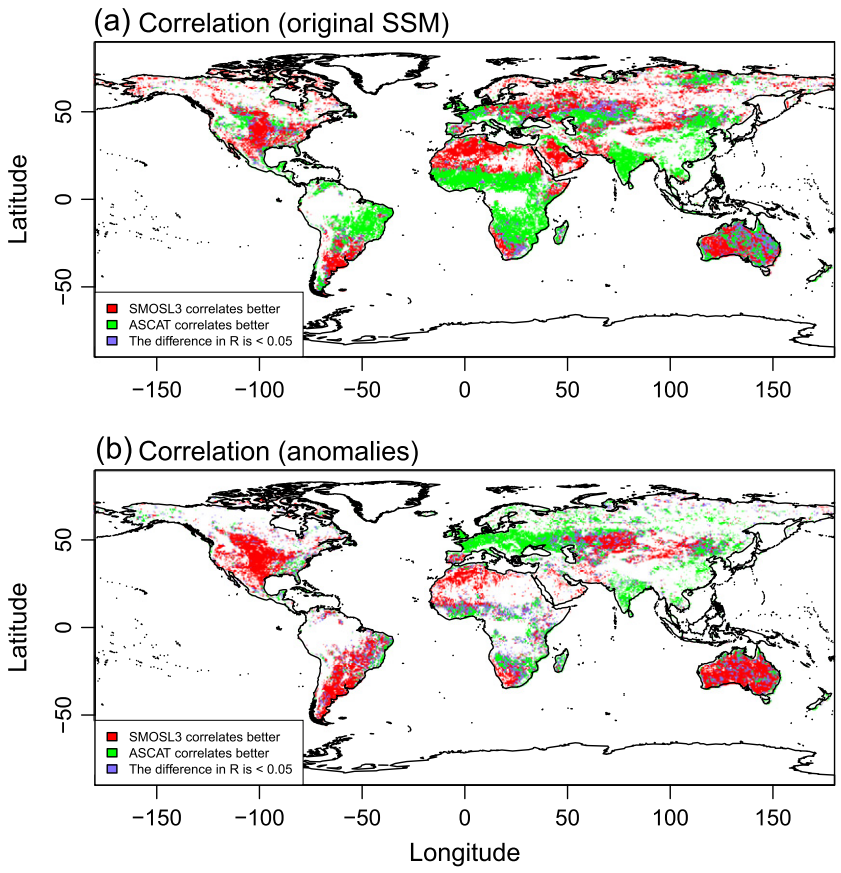

Fig. 5. Pairwise comparison between the ASCAT and SMOSL3 SSM datasets with respect to the reference SSM product in terms of correlations based on the original SSM data (a) or on SSM monthly anomalies (b) during the 05/2010–2012 period. The maps show the areas where either ASCAT (green) or SMOSL3 (red) correlates better with the reference. Pixels where the difference in the values of R is lower than 0.05 appear in blue. Only significant correlations ($p < 0.05$) were plotted and white areas indicate that the correlation is not significant.

Time series correlation values (R) computed for seasonal anomalies, as described in Section 2.3, are shown in Fig. 4c and d. The global spatial patterns are again relatively similar for both SMOSL3 and ASCAT, with a slightly better ability of SMOSL3 to capture the short-term SSM variability of the reference than ASCAT in Central America and Australia, while ASCAT was found to be slightly better in Europe, India, and parts of China. For both datasets, rather high correlation values ($R > 0.5$) with the reference were found in eastern Australia, southern South Africa, Western Europe, and Central America, whereas low values were found in the northern Arabian Peninsula, North Africa, and tundra regions.

Fig. 4e–h shows a similar distribution of ubRMSD and bias values for both SMOSL3 and ASCAT products. The ubRMSD values show a clear spatial distribution: low ubRMSD and bias values were found in deserts (e.g., the Sahara, the Arabian Peninsula, southern South Africa, and central Australia), whereas high values of ubRMSD and bias were found for both instruments in boreal regions, locations near the Equator, and India (only for SMOSL3 because of RFIs).

Due to the model-specific nature of the long-term mean values of soil moisture (Koster et al., 2009), large mean differences (biases) between the remotely sensed and the reference SSM products can be expected. Furthermore, bias may be caused by a wrong estimation of SSM when the satellite footprint includes small water bodies, as was found by (Bartsch, Melzer, Elger, & Heim, 2012; Gouttevin, Bartsch, Krinner, & Naeimi, 2013; Kerr et al., 2012). In Fig. 4g and h, relatively similar bias patterns can be noted for both SMOSL3 and ASCAT at global scale. However, the values of the biases are quite different: in comparison with the MERRA-Land SSM values, higher SSM values can be noted for ASCAT, especially in the boreal regions, whereas lower SSM values can be noted for SMOSL3. The positive bias, found mainly at high latitude regions, in the ASCAT retrievals which is associated to wetter months (i.e. summer periods) can be partially explained by errors in the FAO database used to convert the ASCAT degree of saturation to volumetric water content where values for a few pixels in the northern hemisphere exceed 0.6 m^3/m^3.

Fig. 5a and b compares the areas where SMOSL3 correlates better with the reference than ASCAT (red), and where ASCAT correlates better with the reference than SMOSL3 (green). Looking at original datasets, it can be seen that better correlations with MERRA-Land were obtained with ASCAT over regions with high to moderate vegetation density and in regions where there is a strong seasonality in the SSM variability (e.g., India, Eastern Australia and the North-Central US, locations near the equator). On the other hand, SMOSL3 shows better correlations with MERRA-Land than ASCAT in areas with low to moderate vegetation density (e.g., Western Australia, Sahara, and North America). The latter regions are known to be slightly contaminated by RFI effects (see Fig. 1).

When looking at monthly anomalies (Fig. 5b), ASCAT shows higher correlations with the reference than with SMOSL3 over regions such as Central Europe, China and India, which are known to be highly contaminated by RFI effects (see Fig. 1). With the exception of these regions, SMOSL3 exhibits higher correlations with the reference over most of the grid cells.

3.2. Influence of leaf area index (LAI)

To analyze the effect of vegetation, we computed the average correlation coefficient as a function of the global long term mean LAI, using values of the Global Soil Wetness Project (Dirmeyer et al., 2006). Note that the MERRA-Land simulations use the monthly LAI climatology

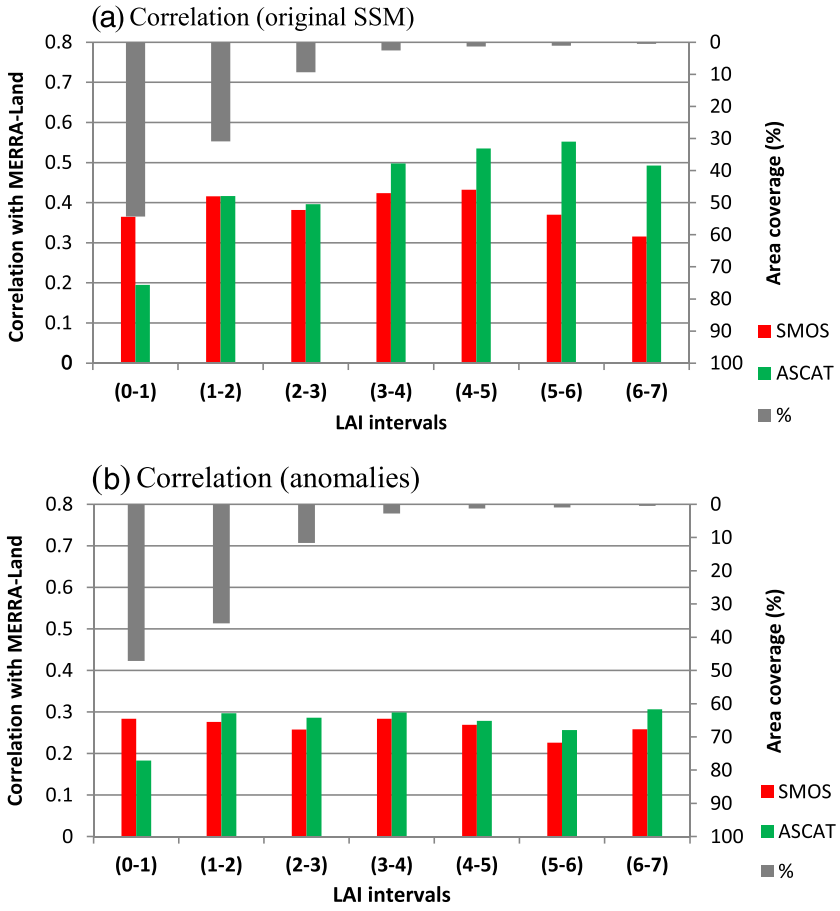

Fig. 6. Distribution of the correlation coefficient (R) between ASCAT (green), SMOSL3 (red) and the reference product (MERRA-Land) for the original SSM data (a) and monthly anomalies (b) as a function of leaf area index (LAI) during the 05/2010–2012 period. Significant correlations ($p < 0.05$) were computed at each grid cell and then averaged by LAI intervals, which were extracted from the global distribution of LAI displayed in Fig. 3. The area coverage provides the cover fraction (%) over continental surfaces corresponding to each LAI interval.

from the Global Soil Wetness Project 2 (GSWP-2). The results for both the original SSM data (Fig. 6a) and the anomalies (Fig. 6b) show that the consistency of the remotely sensed SSM products with the reference (MERRA-Land) is strongly related to LAI. In Fig. 6a, it can be seen that the values of R increase almost linearly with LAI for ASCAT, from $R \approx 0.18$ to $R \approx 0.55$ as LAI increases from about 1 to 7. For SMOSL3, on the other hand, R values remain relatively constant as LAI increases, with values between ~0.32 and 0.44. A decrease in R can be noted for SMOSL3 when LAI is higher than ~4, leading to higher correlation values to the reference with ASCAT, but this corresponds to a very low fraction of the total number of pixels considered here (less than 5%, after screening for uncertain retrievals). In contrast, SMOSL3 provides higher correlation values with the reference than ASCAT when LAI is lower than 1 (i.e. over sparse vegetation covers), which corresponds to almost 50% of the pixels considered in this global analysis, and similar correlation coefficients R are obtained for SMOSL3 and ASCAT for intermediate LAI values ($1 \leq \text{LAI} \leq 3$).

In Fig. 6b, the same analysis is shown for monthly anomalies. As noted above, they exhibit lower correlations to the reference data ($R \approx 0.25$) than the original data, for both SMOSL3 and ASCAT anomalies. The correlation differences between the two remotely sensed products are also much weaker than in Fig. 6a, even if SMOSL3/ASCAT remains better correlated to MERRA-Land for lower/higher values of the LAI.

3.3. Hovmöller diagrams

SSM strongly varies spatially and temporally, and this variability depends mainly on latitude and season (Schlosser & Milly, 2002). It is therefore important to analyze the capability of both ASCAT and SMOSL3 to detect time evolution and spatial patterns of SSM simultaneously. To this end, we used Hovmöller diagrams to illustrate the seasonal variations of SSM for SMOSL3 and ASCAT. The time evolution of the SSM for SMOSL3, ASCAT, and MERRA-Land, averaged along the longitude range by latitude bands, is displayed in Fig. 7. Note that, for SMOSL3, many regions of Europe and Russia are screened out due to RFI contaminations (see Fig. 1), and so the values in the Northern Hemisphere are dominated by estimates from North America. Note also that frozen conditions were excluded from the analysis (see Section 2.2), so there is no-data at latitudes above 55°N in the winter time. The main difference between the three HDs is a difference in mean, with higher SSMs according to MERRA-Land. This is consistent with the negative biases of the remotely sensed SSM products with respect to the MERRA-Land reference shown in Fig. 4g–h. Moreover, Fig. 7 reveals a common periodical behavior with time and latitude: the lowest values are comprised in two "parallel" sinusoidal bands around the equator reaching the minima around April. Hence, ASCAT and SMOSL3 capture the SSM seasonal variations in the inter-tropical area as simulated by MERRA-Land. The meridional shift of the Intertropical Convergence Zone (ITCZ) is well detected by all three datasets, but MERRA-Land presents higher seasonal cycle variations.

The main differences in the SSM distribution are found in the Northern Hemisphere particularly related to the increase of SSM values during the summer period. Furthermore, very low SMOS SSM values (bright red color in Fig. 7c, i.e., SSM values close to 0.05 m^3/m^3) can be noted north of ~50°N during the winter. It is likely these very low values can be explained by the effect of soil freezing: the SMOS sensor cannot distinguish between frozen and very dry soil conditions as the real

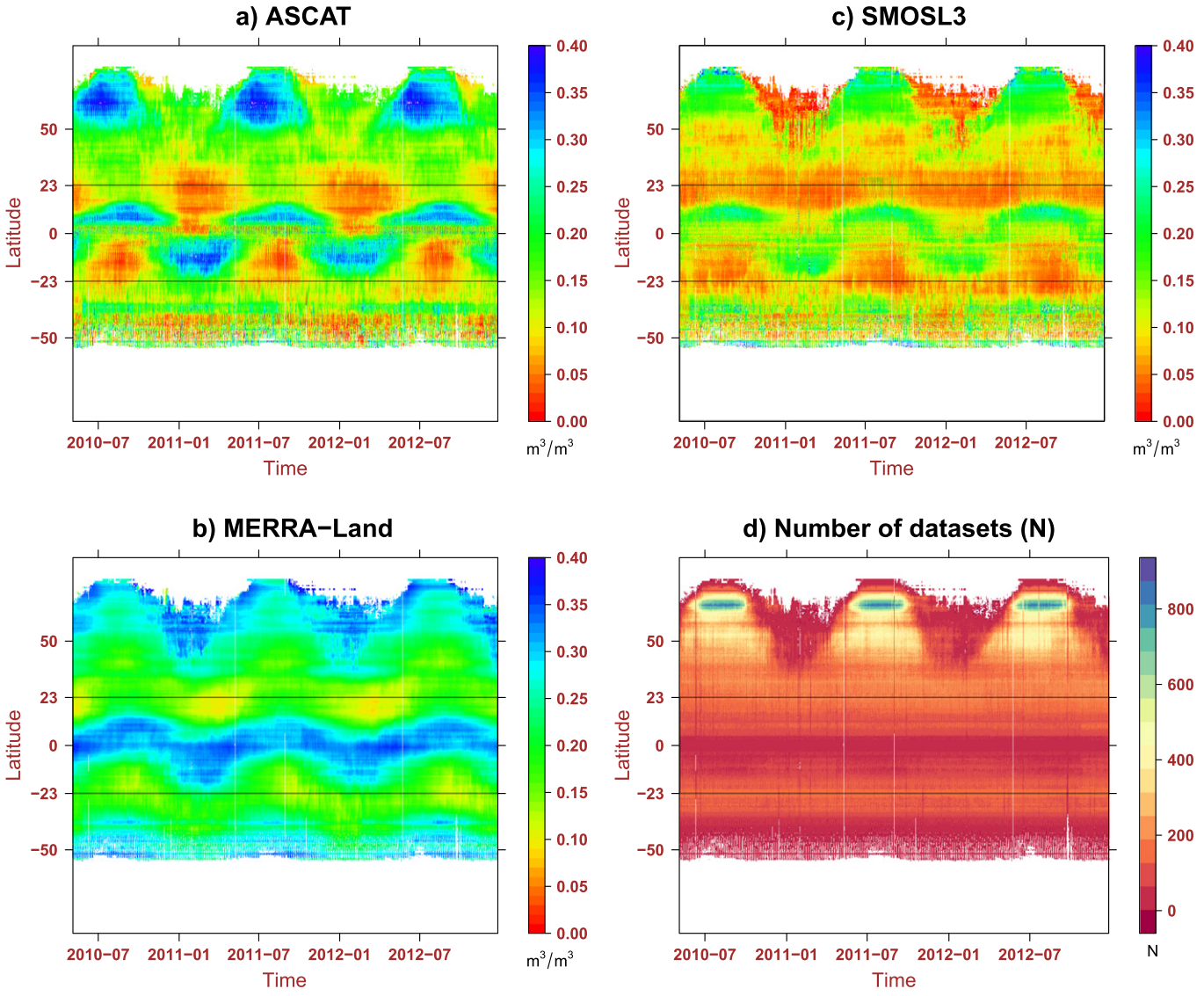

Fig. 7. Time–latitude variations of original surface soil moisture data (m^3/m^3) for (a) ASCAT, (b) MERRA-L, (c) SMOSL3 and (d) number of data illustrated in Hovmöller diagrams.

part of the permittivity for both conditions are very close (values of permittivity ~5; Wigneron et al., 2007). So, it is likely that frozen soil conditions were not correctly flagged and excluded in the SMOSL3 products, and that the screening based on MERRA-Land soil temperatures may not be sufficient. For the same reasons, unrealistically drier winter-time SSM conditions were also retrieved by ASCAT in the same northern regions, albeit to a lower extent than for SMOS, with SSM values close to 0.2 m^3/m^3. Conversely, MERRA-Land SSM includes both liquid and frozen water and therefore shows a more realistic increase in SSM during the winter. These results show that correctly detecting and screening frost and snow is still a big challenge.

3.4. Triple collocation error model

Global error maps for the remotely sensed SSM long-term anomalies (excluding the effect of the biases) are derived using the TCE method over the 2010–2012 period. Fig. 8a and b illustrates the TCE errors (i.e. the square-root of the values obtained from Eqs. (13)–(14)) of SMOSL3 and ASCAT.

In general, the spatial patterns of the TCE errors obtained with ASCAT and SMOS are similar with relatively low TCE errors, with a mean global error of 0.014 m^3/m^3 for SMOSL3, and 0.015 m^3/m^3 for ASCAT. Note that the mean global error found for SMOSL3 in our study is much lower than the one found by Leroux et al. (2011) (~0.06 m^3/m^3). The higher mean value obtained by Leroux et al. may be explained by the use of only one year (2010), while we used 3 years in the present analysis (2010–2012). Also, Leroux et al. (2011) did not exclude SSM data measured during the commissioning phase which might have increased the error for the SMOS dataset. Moreover, the way to handle data filtering using flags such as the data quality index and RFI percentage may be different in both studies.

As shown in Fig. 8a and b, the error estimates for both products are lowest in arid regions (e.g., Arabian Peninsula, Central Australia, and Egypt) due to low amounts of precipitation received leading to a low temporal variability of SSM in these regions. Higher TCE errors were found for both SMOSL3 and ASCAT over India and over locations near the Equator (e.g., South Sudan, Zambia) where MERRA-Land is much less reliable due to the paucity of precipitation gauges, particularly over most of the African continent.

Relatively high errors were obtained for ASCAT in some arid regions (e.g., Algeria, Libya, and Iran) which is a well-known phenomenon already noted in the previous Sections (3.1 and 3.2). Fig. 9 shows the areas where SMOSL3 provided lower errors than ASCAT (red), where ASCAT provided lower errors than SMOSL3 (green). Note that the absolute magnitude of the estimated error depends on the TCE reference. In general, it can be seen that lowest errors were obtained with ASCAT

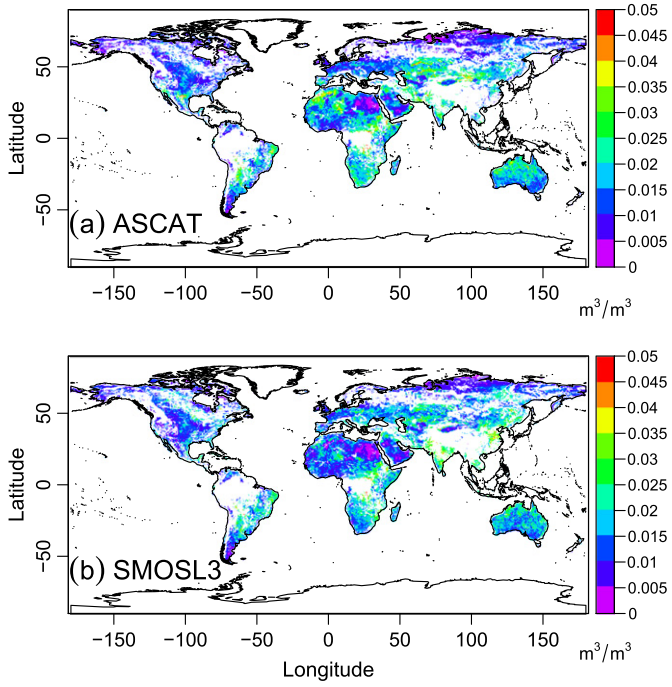

Fig. 8. Spatial TCE errors of (a) ASCAT and (b) SMOSL3 SSM estimates expressed in volumetric water content. White areas indicate areas for which less than 100 common observations were available.

over regions with high to moderate vegetation density, and in regions where there is a strong seasonality in the SSM variability (e.g., India, in parts of Amazonia, Central Europe, Eastern Australia and the North-Eastern USA). On the other hand lower errors were obtained with SMOSL3 in areas with low to moderate vegetation density (e.g., Western Australia, Sahara, and western US, Central Asia), confirming the results shown in the previous section about the sensitivity to the vegetation effects.

4. Discussion and conclusions

4.1. Summary of the results

This study investigated the consistency of two microwave-based SSM products with respect to a reference SSM product, namely the MERRA-Land SSM product, derived from the MERRA reanalysis, for the period 05/2010–12/2012 at the global scale. The two remote sensing products are (i) the SMOSL3 SSM product, which is a microwave-based product derived from L-band passive brightness temperature measurements developed and supported by the CATDS, and (ii) the ASCAT SSM product, which is a microwave-based product derived from C-band active backscatter measurements, developed and supported by TU-Wien.

The analysis of the original data shows, in general, a good correspondence between the SMOSL3 and ASCAT derived SSM products with the MERRA-Land reference. For instance, SMOSL3 and ASCAT successfully captured the spatio-temporal dynamics of the MERRA-Land SSM product, as seen in the correlation analyses, in the transition zones between wet and dry climates (e.g., Great Plains of North America, Sahel), Eastern Australia, and South-eastern regions of Brazil. It is worth noting that the regions of good agreement between SMOSL3, ASCAT, and MERRA-Land are also regions of strong coupling between soil moisture and precipitation as demonstrated by Koster et al. (2004).

SMOSL3 and ASCAT exhibited weak correlations with the MERRA-Land reference data in tundra and arid regions (e.g., Sahara, Arabian Peninsula, and central Australia). ASCAT even exhibited negative correlations over some of the dry deserts (e.g., Sahara). These low correlations may be explained by the small range of variation in the SSM values in these dry regions which corresponds roughly to the remotely sensed retrieval accuracy (~0.04 m^3/m^3, Kerr et al., 2001). Issues with the ASCAT SSM retrievals in dry regions may be explained by (i) systematic errors in the retrieval algorithm due to different scattering mechanisms in dry soils (Wagner et al., 2013) and (ii) changes in small-scale surface roughness, produced by wind-blown sand (Frison & Mougin, 1996). Anomaly time series correlations show, in general, similar spatial patterns compared to the correlations found using original datasets, but with lower *R* values, especially in the transition zones.

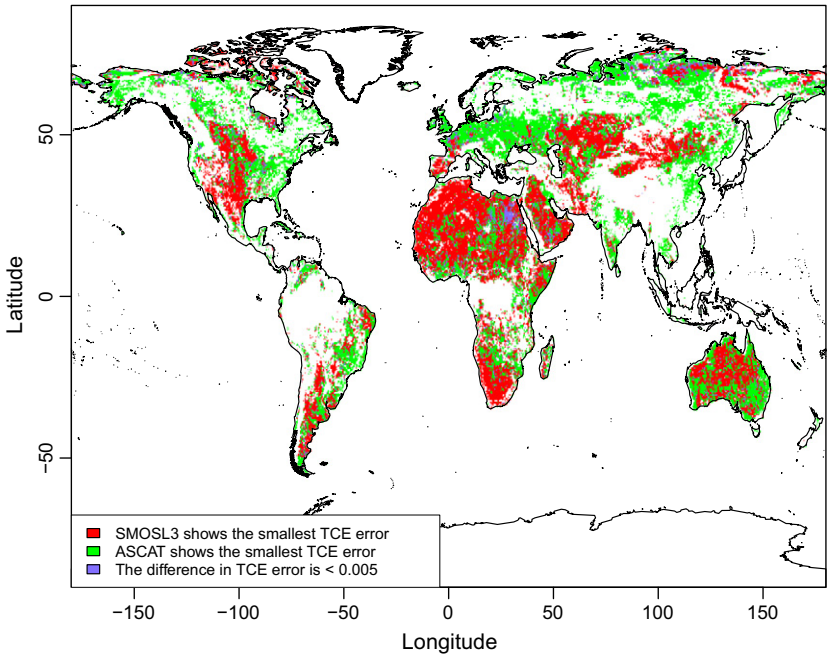

Fig. 9. The areas in which either ASCAT (green) or SMOSL3 (red) shows the smallest TCE error value. Pixels where the difference in TCE error is less than 0.005 m^3/m^3 appear in blue. White areas indicate areas for which less than 100 common observations were available.

The global scale analysis of the bias and ubRMSD also confirmed these results. However, opposite patterns were generally obtained in terms of bias: ASCAT is generally wetter than MERRA-Land (positive bias), while SMOSL3 is generally drier than MERRA-Land (negative bias).

Additional insights were provided by the Hovmöller diagrams, which visualize the time changes in SSM as a function of latitude. It is found that even though strong correlations are found between all three products at global scale, the spatio-temporal patterns shown in the HD may be quite different for SMOSL3, ASCAT and MERRA-Land in some latitudinal bands. For instance, SMOSL3 presents consistently dry SSM conditions (less than ~0.10 m^3/m^3) at mid latitudes (between 10°N and 30°N). This could be partly explained by the impact of RFI as high RFI values increase the SMOS observed brightness temperatures (TB) resulting in lower SSM retrievals (Oliva et al., 2012). Wigneron, Schwank, Lopez Baeza, Kerr, et al. (2012) have interpreted the bias as an effect of the underestimation of the default contribution to TB of the forested areas in mixed pixels.

Finally, results from the TCE method generally confirmed the above results and the spatial error patterns were found to be consistent with known performance issues of SMOS and ASCAT (Leroux et al., 2013). In particular, larger errors were found for SMOSL3 in the presence of moderate to dense vegetation in tropical and temperate regions and in regions known to be highly contaminated by RFI effects (Western Europe, India, Southern Asia). Higher errors were found for ASCAT over arid regions (North Africa, Central Australia, and central Asia). Our findings are generally in agreement with the results obtained by previous studies analyzing spatial errors of ASCAT over 2007–2008 (e.g., Dorigo et al., 2010; Hain, Crow, Mecikalski, Anderson, & Holmes, 2011; Leroux et al., 2011; Miralles et al., 2010; Parinussa et al., 2011) and SMOS over 2010 (Leroux et al., 2011), using products based on earlier versions of the retrieval algorithms.

A more in-depth analysis, using LAI as a parameter to quantify the vegetation effects, revealed higher *R* values for SMOSL3 than for ASCAT when LAI is less than 1 (which corresponds to almost 50% of the pixels considered in this study), similar *R* values for both products for intermediate LAI values between 1 and 3, and higher *R* values for ASCAT than for SMOS when LAI exceeds 3. This implies that vegetation plays a key role in the performance of the SMOSL3 and ASCAT SSM products, and that the two products have different sensitivities to vegetation. Generally, SMOS is more efficient at monitoring SSM than ASCAT over sparse vegetation, whereas ASCAT is more efficient over relatively dense vegetation (LAI >3).

4.2. Discussion

These results may appear as surprising because microwave sensors should be more efficient to sense through moderate vegetation at L-band than at C-band (Al-Yaari et al., 2014): with increasing frequency (i) scattering and attenuation effects by vegetation elements (leaves, stems, trunks, branches, fruits, etc.) increase and (ii) the sampling depth in soil decreases. However, in this study, SMOS and ASCAT differ not only in terms of frequency but also in terms of microwave technology: SMOS is a radiometer (i.e. a passive microwave system), while ASCAT is a scatterometer (i.e. an active microwave system). Previous studies comparing SSM retrievals from radiometer and scatterometer systems (Brocca et al., 2011; Rüdiger et al., 2009) also found that SSM products retrieved from scatterometer data were less impacted by vegetation than those retrieved from radiometers data.

There are different ways of interpreting these results. First, the good performances of ASCAT over vegetation canopies could be due to higher-order surface-vegetation interaction effects (Crow, Wagner, & Naeimi, 2010), such as double bounce reflection (Karam et al., 1995) that may increase the sensitivity of active systems to SSM in comparison to passive systems. These higher-order effects are often neglected in the current models used for SSM retrievals from both active and passive systems. However, these interaction effects may become extremely important under some conditions and may, to a large extent, explain the sensitivity of ASCAT to soil moisture over vegetated regions even at high incidence angles (Crow et al., 2010).

Second, the scatterometer systems have been also found to be very sensitive to the seasonal vegetation dynamics. For instance, early studies which investigated signatures from ERS backscatter coefficients based on averaged observations on a monthly basis have shown that the time variations in the measured backscatter coefficient were in good agreement with the vegetation dynamics as monitored by optical vegetation indices (Frison & Mougin, 1996). It should be noted that, for some specific conditions, the increase in vegetation effects and the increase in SSM both lead to an increase in the backscatter coefficient (Wigneron, Ferrazzoli, Calvet, & Bertuzzi, 1999; Wigneron, Ferrazzoli, Olioso, Bertuzzi, & Chanzy, 1999), which may make the decoupling of the two effects difficult using an active system such as ASCAT. So, it is difficult to appreciate whether ASCAT is really monitoring the time variations in SSM or in the vegetation in regions where there is a natural high correlation between the vegetation dynamics and the increase in the SSM values. The hypothesis that ASCAT may have difficulties in decoupling vegetation and SSM effects at the seasonal scale may be used to interpret the fact that the performances of ASCAT become closer to those of SMOSL3 for LAI > 3 when anomalies (taking off seasonal effects) were used (Fig. 6a and b).

However, many results can be raised to contradict this hypothesis. For instance, in many climate regions (Mediterranean Climate regions for instance) where soil moisture and vegetation may be out of phase, ASCAT performed quite well. Moreover, the increase in vegetation density often leads to an increase in backscatter, but the opposite may also happen, depending on the soil moisture conditions. Eventually, considering anomalies, the performances of SMOS and ASCAT were very close (ASCAT slightly better) in terms of correlation values for LAI > 1. This latter result confirms the very good ability of active systems such as ASCAT in monitoring SSM over well-developed vegetation.

It is also important to keep in mind that MERRA-Land, although found to be very reliable in several instances (Albergel, Dorigo, Reichle, et al., 2013; Yi et al., 2011), cannot be considered to be "ground truth" (Albergel, Dorigo, Balsamo, et al., 2013). Consequently, the interpretation of the results depends on the accuracy of the MERRA-Land product itself. The skill of MERRA-Land soil moisture strongly depends on the accuracy of the precipitation forcing, which is derived by merging the MERRA reanalysis precipitation with measurements from a global network of gauges. The density of the gauge network varies tremendously, with good coverage in North America, Europe and many parts of Asia and South America. However, the gauge density is very sparse in Africa and at high latitudes. In these regions in particular, a lack of consistency between the remote sensing products and MERRA-Land SSM does not necessarily imply poor performance by the remote sensing estimates. Other factors that determine the skill of MERRA-Land soil moisture include the radiation forcing as well as the land model physics and associated model parameters, whose quality is similarly variable across the globe.

Looking ahead, improvements in the retrieval algorithms as well as in the LSM data can be expected. For the SMOSL3 product, this includes enhancements especially in terms of RFI filtering and dry bias correction. For ASCAT, the issues found over arid regions are currently under investigation. Finally, the next version of the MERRA reanalysis is currently in production and features improved precipitation forcing, the single most critical input to SSM estimates from models.

The results of the present study revealed that both the SMOSL3 and the ASCAT SSM products are largely consistent with the model-based SSM estimates from MERRA-Land, and that the two remote sensing products complement each other. Vegetation density and RFI contaminations of SMOSL3 were found to be the key factors in the interpretation of the consistency between the two remotely sensed products (SMOSL3 and ASCAT) with MERRA-Land. The potential synergy between the

passive and active microwave systems at global scale is very promising for the development of improved, long-term SSM time series at global scale, such as those pursued by the European Space Agency's Climate Change Initiative.

Acknowledgments

This research work was funded by the TOSCA (Terre Océan Surfaces Continentales et Atmosphère) CNES program and the Islamic Development Bank (IDB). Gabrielle De Lannoy and Rolf Reichle were supported by the NASA Soil Moisture Active Passive mission. The authors acknowledge CATDS for the SMOSL3 dataset (http://catds.ifremer.fr) and the Vienna University of Technology (TU-WIEN) for the ASCAT product. SMOS team at CESBIO is thanked for fruitful discussions. Mr Christophe Moisy provided valuable technical assistance.

References

Al Bitar, A., Leroux, D., Kerr, Y. H., Merlin, O., Richaume, P., Sahoo, A., et al. (2012). Evaluation of SMOS soil moisture products over continental U.S. using the SCAN/SNOTEL network. *IEEE Transactions on Geoscience and Remote Sensing, 50*, 1572–1586.

Albergel, C., de Rosnay, P., Gruhier, C., Munoz-Sabater, J., Hasenauer, S., Isaksen, L., et al. (2012). Evaluation of remotely sensed and modelled soil moisture products using global ground-based in situ observations. *Remote Sensing of Environment, 118*, 215–226.

Albergel, C., Dorigo, W., Balsamo, G., Muñoz-Sabater, J., de Rosnay, P., Isaksen, L., et al. (2013a). Monitoring multi-decadal satellite earth observation of soil moisture products through land surface reanalyses. *Remote Sensing of Environment, 138*, 77–89.

Albergel, C., Dorigo, W., Reichle, R. H., Balsamo, G., de Rosnay, P., Muñoz-Sabater, J., et al. (2013b). Skill and global trend analysis of soil moisture from reanalyses and microwave remote sensing. *Journal of Hydrometeorology, 14*, 1259–1277.

Albergel, C., Rüdiger, C., Carrer, D., Calvet, J. -C., Fritz, N., Naeimi, V., et al. (2009). An evaluation of ASCAT surface soil moisture products with in-situ observations in Southwestern France. *Hydrology and Earth System Sciences, 13*.

Alyaari, A., Wigneron, J., Ducharne, A., Kerr, Y., Al Bitar, A., de Jeu, R., et al. (2014). Global-scale evaluation of two satellite-based passive microwave soil moisture datasets (SMOS and AMSR-E) with respect to modelled estimates. *13th Specialist Meeting on Microwave Radiometry and Remote Sensing of the Environment*.

Al-yaari, A., Wigneron, J. -P., Ducharne, A., Kerr, Y., de Rosnay, P., de Jeu, R., et al. (2014). Global- scale evaluation of two satellite-based passive microwave soil moisture datasets (SMOS and AMSR-E) with respect to Land Data Assimilation System estimates. *Remote Sensing of Environment, 149*, 181–195.

Balsamo, G., Viterbo, P., Beljaars, A.C. M., van den Hurk, B. J. J. M., Hirschi, M., Betts, A. K., et al. (2009). A revised hydrology for the ECMWF model: Verification from field site to terrestrial water storage and impact in the ECMWF-IFS. *Journal of Hydrometeorology, 10*.

Barichivich, J., Briffa, K., Myneni, R., Schrier, G., Dorigo, W., Tucker, C., et al. (2014). Temperature and snow-mediated moisture controls of summer photosynthetic activity in northern terrestrial ecosystems between 1982 and 2011. *Remote Sensing, 6*, 1390–1431.

Bartalis, Z., Wagner, W., Naeimi, V., Hasenauer, S., Scipal, K., Bonekamp, H., et al. (2007). Initial soil moisture retrievals from the METOP-A Advanced Scatterometer (ASCAT). *Geophysical Research Letters, 34*, L20401.

Bartsch, A., Melzer, T., Elger, K., & Heim, B. (2012). Soil Moisture from Metop ASCAT Data at High Latitudes. In K. Hinckel (Ed.), *Tenth International Conference on Permafrost (TICOP)* (pp. 33–38).

Brocca, L., Hasenauer, S., Lacava, T., Melone, F., Moramarco, T., Wagner, W., et al. (2011). Soil moisture estimation through ASCAT and AMSR-E sensors: An intercomparison and validation study across Europe. *Remote Sensing of Environment, 115*, 3390–3408.

Brocca, L., Melone, F., Moramarco, T., Wagner, W., & Hasenauer, S. (2010). ASCAT soil wetness index validation through in situ and modeled soil moisture data in central Italy. *Remote Sensing of Environment, 114*, 2745–2755.

CECR (2012). Comprehensive Error Characterisation Report, Version 0.7. *ESA Climate Change Initiative Phase 1 Soil Moisture Project*.

Crow, W. T., Wagner, W., & Naeimi, V. (2010). The impact of radar incidence angle on soil-moisture-retrieval skill. *IEEE Geoscience and Remote Sensing Letters, 7*, 501–505.

Daly, E., & Porporato, A. (2005). A review of soil moisture dynamics: From rainfall infiltration to ecosystem response. *Environmental Engineering Science, 22*(1), 9–24.

Dirmeyer, P. A., Gao, X., Zhao, M., Zhichang, G., Oki, T., & Hanasaki, N. (2006). GSWP¬ 2: Multimodel analysis and implications for our perception of the land surface. *American Meteorological B, 87*.

Dorigo, W., de Jeu, R., Chung, D., Parinussa, R., Liu, Y., Wagner, W., et al. (2012). Evaluating global trends (1988–2010) in harmonized multi-satellite surface soil moisture. *Geophysical Research Letters, 39*, L18405.

Dorigo, W. A., Scipal, K., Parinussa, R. M., Liu, Y. Y., Wagner, W., de Jeu, R. A.M., et al. (2010). Error characterisation of global active and passive microwave soil moisture datasets. *Hydrology and Earth System Sciences, 14*, 2605–2616.

Draper, C., Mahfouf, J. F., Calvet, J. C., Martin, E., & Wagner, W. (2011). Assimilation of ASCAT near-surface soil moisture into the SIM hydrological model over France. *Hydrology and Earth System Sciences, 15*, 3829–3841.

Draper, C., Reichle, R., de Jeu, R., Naeimi, V., Parinussa, R., & Wagner, W. (2013). Estimating root mean square errors in remotely sensed soil moisture over continental scale domains. *Remote Sensing of Environment, 137*, 288–298.

Draper, C. S., Reichle, R. H., De Lannoy, G. J. M., & Liu, Q. (2012). Assimilation of passive and active microwave soil moisture retrievals. *Geophysical Research Letters, 39*, L04401.

Entekhabi, D., Njoku, E. G., O'Neill, P. E., Kellogg, K. H., Crow, W. T., Edelstein, W. N., et al. (2010). The Soil Moisture Active Passive (SMAP) Mission. *Proceedings of the IEEE, 98*, 704–716.

FAO (2003). Digital soil map of the world (DSMW). *Tech. rep., Food and Agriculture Organization of the United Nations* (Re-issued version).

Frison, P. L., & Mougin, E. (1996). Monitoring global vegetation dynamics with ERS-1 wind scatterometer data. *International Journal of Remote Sensing, 17*, 3201–3218.

Gouttevin, I., Bartsch, A., Krinner, G., & Naeimi, V. (2013). A comparison between remotely-sensed and modelled surface soil moisture (and frozen status) at high latitudes. *Hydrology and Earth System Sciences Discussions, 10*, 11241–11291.

Hain, C. R., Crow, W. T., Mecikalski, J. R., Anderson, M. C., & Holmes, T. (2011). An intercomparison of available soil moisture estimates from thermal infrared and passive microwave remote sensing and land surface modeling. *Journal of Geophysical Research, [Atmospheres], 116*, D15107.

Hovmöller, E. (1949). The trough-and-ridge diagram. *Tellus, 1*, 62–66.

Jacquette, E., Al Bitar, A., Mialon, A., Kerr, Y., Quesney, A., Cabot, F., et al. (2010). *SMOS CATDS level 3 global products over land.* (78240K-78240K).

Janssen, P. A. E. M., Abdalla, S., Hersbach, H., & Bidlot, J. -R. (2007). Error estimation of buoy, satellite, and model wave height data. *Journal of Atmospheric and Oceanic Technology, 24*, 1665–1677.

Karam, M.A., Amar, F., Fung, A. K., Mougin, E., Lopes, A., Le Vine, D.M., et al. (1995). A microwave polarimetric scattering model for forest canopies based on vector radiative transfer theory. *Remote Sensing of Environment, 53*, 16–30.

Kerr, Y. (2007). Soil moisture from space: Where are we? *Hydrogeology Journal, 15*, 117–120.

Kerr, Y., Jacquette, E., Al Bitar, A., Cabot, F., Mialon, A., Richaume, P., et al. (2013a). *The CATDS SMOS L3 soil moisture retrieval processor.* Algorithm Theoretical Baseline Document (ATBD). *SO-TN-CBSA-GS-0029*.

Kerr, Y., Richaume, P., Waldteufel, P., Wigneron, J. P., Ferrazzoli, P., & Mahmoodi, A. (2013b). *SMOS level 2 Processor for Soil Moisture ATBD.* ESA No: SO-TN-ESL-SM-GS-0001.

Kerr, Y. H., Waldteufel, P., Richaume, P., Wigneron, J. P., Ferrazzoli, P., Mahmoodi, A., et al. (2012). The SMOS soil moisture retrieval algorithm. *IEEE Transactions on Geoscience and Remote Sensing, 50*, 1384–1403.

Kerr, Y. H., Waldteufel, P., Wigneron, J. P., Delwart, S., Cabot, F., Boutin, J., et al. (2010). The SMOS Mission: New Tool for Monitoring Key Elements ofthe Global Water Cycle. *Proceedings of the IEEE, 98*, 666–687.

Kerr, Y. H., Waldteufel, P., Wigneron, J. P., Martinuzzi, J., Font, J., & Berger, M. (2001). Soil moisture retrieval from space: The Soil Moisture and Ocean Salinity (SMOS) mission. *IEEE Transactions on Geoscience and Remote Sensing, 39*, 1729–1735.

Koster, R. D., Dirmeyer, P. A., Guo, Z., Bonan, G., Chan, E., Cox, P., et al. (2004). Regions of strong coupling between soil moisture and precipitation. *Science, 305*, 1138–1140.

Koster, R. D., Guo, Z., Yang, R., Dirmeyer, P. A., Mitchell, K., & Puma, M. J. (2009). On the nature of soil moisture in land surface models. *Journal of Climate, 22*, 4322–4335.

Leroux, D. J., Kerr, Y. H., Richaume, P., & Berthelot, B. (2011). Estimating SMOS error structure using triple collocation. *Geoscience and Remote Sensing Symposium (IGARSS), 2011 IEEE International* (pp. 24–27).

Leroux, D. J., Kerr, Y. H., Richaume, P., & Fieuzal, R. (2013). Spatial distribution and possible sources of SMOS errors at the global scale. *Remote Sensing of Environment, 133*, 240–250.

Liu, Y. Y., Dorigo, W. A., Parinussa, R. M., de Jeu, R. A.M., Wagner, W., McCabe, M. F., et al. (2012). Trend-preserving blending of passive and active microwave soil moisture retrievals. *Remote Sensing of Environment, 123*, 280–297.

Liu, Y. Y., Parinussa, R. M., Dorigo, W. A., De Jeu, R. A.M., Wagner, W., van Dijk, A. I. J. M. , et al. (2011). Developing an improved soil moisture dataset by blending passive and active microwave satellite-based retrievals. *Hydrology and Earth System Sciences, 15*.

Loew, A., & Schlenz, F. (2011). A dynamic approach for evaluating coarse scale satellite soil moisture products. *Hydrology and Earth System Sciences, 15*, 75–90.

Loew, A., Stacke, T., Dorigo, W., de Jeu, R., & Hagemann, S. (2013). Potential and limitations of multidecadal satellite soil moisture observations for selected climate model evaluation studies. *Hydrology and Earth System Sciences, 17*, 3523–3542.

Miralles, D.G., Crow, W. T., & Cosh, M. H. (2010). Estimating spatial sampling errors in coarse-scale soil moisture estimates derived from point-scale observations. *Journal of Hydrometeorology, 11*, 1423–1429.

Miralles, D.G., van den Berg, M. J., Gash, J. H., Parinussa, R. M., de Jeu, R. A.M., Beck, H. E., et al. (2014). El Niño–La Niña cycle and recent trends in continental evaporation. *Nature Climate Change, 4*, 122–126.

Naeimi, V., Scipal, K., Bartalis, Z., Hasenauer, S., & Wagner, W. (2009). An improved soil moisture retrieval algorithm for ERS and METOP scatterometer observations. *IEEE Transactions on Geoscience and Remote Sensing, 47*, 1999–2013.

Njoku, E. G., Ashcroft, P., Chan, T. K., & Li, L. (2005). Global survey and statistics of radio-frequency interference in AMSR-E Land observations. *IEEE Transactions on Geoscience and Remote Sensing, 46*.

Njoku, E. G., Jackson, T. J., Lakshmi, V., Chan, T. K., & Nghiem, S. V. (2003). Soil moisture retrieval from AMSR-E. *IEEE Transactions on Geoscience and Remote Sensing, 41*, 215–229.

Oliva, R., Daganzo, E., Kerr, Y. H., Mecklenburg, S., Nieto, S., Richaume, P., et al. (2012). SMOS radio frequency interference scenario: Status and actions taken to improve the RFI environment in the 1400–1427-MHz passive band. *IEEE Transactions on Geoscience and Remote Sensing, 50*, 1427–1439.

Owe, M., de Jeu, R., & Holmes, T. (2008). Multisensor historical climatology of satellite-derived global land surface moisture. *Journal of Geophysical Research Earth Surface*, *113*, F01002.

Parinussa, R., Meesters, A., Liu, Y., Dorigo, W., Wagner, W., & de Jeu, R. (2011). An analytical solution to estimate the error structure of a global soil moisture dataset. *IEEE Geoscience and Remote Sensing Letters*, *8*, 779–783.

Parrens, M., Zakharova, E., Lafont, S., Calvet, J. C., Kerr, Y., Wagner, W., et al. (2012). Comparing soil moisture retrievals from SMOS and ASCAT over France. *Hydrology and Earth System Sciences*, *16*, 423–440.

Reichle, R. H. (2012). The MERRA-Land Data Product. *GMAO Office Note No. 3* ((Version 1.2), 38 pp).

Reichle, R. H., Koster, R. D., De Lannoy, G. J. M., Forman, B.A., Liu, Q., Mahanama, S. P. P., et al. (2011). Assessment and enhancement of MERRA land surface hydrology estimates. *Journal of Climate*, *24*, 6322–6338.

Rienecker, M. M., Suarez, M. J., Gelaro, R., Todling, R., Bacmeister, J., Liu, E., et al. (2011). MERRA: NASA's modern-era retrospective analysis for research and applications. *Journal of Climate*, *24*, 3624–3648.

Rüdiger, C., Calvet, J. -C., Gruhier, C., Holmes, T. R. H., de Jeu, R. A.M., & Wagner, W. (2009). An intercomparison of ERS-Scat and AMSR-E soil moisture observations with model simulations over France. *Journal of Hydrometeorology*, *10*.

Sanchez, N., Martinez-Fernandez, J., Scaini, A., & Perez-Gutierrez, C. (2012). Validation of the SMOS L2 soil moisture data in the REMEDHUS network (Spain). *IEEE Transactions on Geoscience and Remote Sensing*, *50*, 1602–1611.

Schlosser, C. A., & Milly, P. C. D. (2002). A model-based investigation of soil moisture predictability and associated climate predictability. *Journal of Hydrometeorology*, *3*, 483–501.

Scipal, K., Dorigo, W., & de Jeu, R. (2010). Triple collocation—a new tool to determine the error structure of global soil moisture products. *Geoscience and Remote Sensing Symposium (IGARSS), 2010 IEEE International* (pp. 4426–4429).

Scipal, K., Drusch, M., & Wagner, W. (2008). Assimilation of a ERS scatterometer derived soil moisture index in the ECMWF numerical weather prediction system. *Advances in Water Resources*, *31*, 1101–1112.

Scipal, K., Holmes, T., de Jeu, R., Naeimi, V., & Wagner, W. (2008). A possible solution for the problem of estimating the error structure of global soil moisture datasets. *Geophysical Research Letters*, *35*, L24403.

Seneviratne, S. I., Luthi, D., Litschi, M., & Schar, C. (2006). Land-atmosphere coupling and climate change in Europe. *Nature*, *443*, 205–209.

Sinclair, S., & Pegram, G. G. S. (2010). A comparison of ASCAT and modelled soil moisture over South Africa, using TOPKAPI in land surface mode. *Hydrology and Earth System Sciences*, *14*.

Stoffelen, A. (1998). Toward the true near-surface wind speed: Error modeling and calibration using triple collocation. *Journal of Geophysical Research Oceans*, *103*, 7755–7766.

Su, Z., Wen, J., Dente, L., van der Velde, R., Wang, L., Ma, Y., et al. (2011). The Tibetan Plateau observatory of plateau scale soil moisture and soil temperature (Tibet-Obs) for quantifying uncertainties in coarse resolution satellite and model products. *Hydrology and Earth System Sciences*, *15*.

System G.C.O. (2010). *Implementation plan for the Global Observing System for climate in support of the UNFCC (2010 Update)*. (180 pp).

Taylor, C. M., de Jeu, R. A.M., Guichard, F., Harris, P. P., & Dorigo, W. A. (2012). Afternoon rain more likely over drier soils. *Nature*, *489*, 423–426.

Wagner, W., Bloeschl, G., Pampaloni, P., Calvet, J. -C., Bizzarri, B., Wigneron, J. -P., et al. (2007). Operational readiness of microwave remote sensing of soil moisture for hydrologic applications. *Nordic Hydrology*, *38*, 1–20.

Wagner, W., Hahn, S., Kidd, R., Melzer, T., Bartalis, Z., Hasenauer, S., et al. (2013). The ASCAT soil moisture product: A review of its specifications, validation results, and emerging applications. *Meteorologische Zeitschrift*, *22*, 5–33.

Wagner, W., Lemoine, G., & Rott, H. (1999). A method for estimating soil moisture from ERS scatterometer and soil data. *Remote Sensing of Environment*, *70*, 191–207.

Western, A. W., Grayson, R. B., & Blöschl, G. (2002). Scaling of soil moisture: A hydrologic perspective. *Annual Review of Earth and Planetary Sciences*, *30*, 149–180.

Wigneron, J. -P., Ferrazzoli, P., Calvet, J. C., & Bertuzzi, P. (1999). A parametric study on passive and active microwave observations over a soybean crop. *IEEE Transactions on Geoscience and Remote Sensing*, *37*, 2728–2733.

Wigneron, J. -P., Ferrazzoli, P., Olioso, A., Bertuzzi, P., & Chanzy, A. (1999). A simple approach to monitor crop biomass from C-band radar data. *Remote Sensing of Environment*, *69*(179–188), 1999.

Wigneron, J. -P., Kerr, Y., Waldteufel, P., Saleh, K., Escorihuela, M. J., Richaume, P., et al. (2007). L-band microwave emission of the biosphere (L-MEB) model: description and calibration against experimental datasets over crop fields. *Remote Sensing of Environment*, *107*, 639–655.

Wigneron, J. -P., Schwank, M., Lopez Baeza, E., Kerr, Y. H., Novello, N., Millan, C., et al. (2012). First evaluation of the SMOS observations over the VAS site in the Mediterranean region. *Remote Sensing Environment*, *124*, 26–37.

Wigneron, J. -P., Waldteufel, P., Chanzy, A., Calvet, J. C., & Kerr, Y. (2000). Two-dimensional microwave interferometer retrieval capabilities over land surfaces (SMOS Mission). *Remote Sensing of Environment*, *73*, 270–282.

Yi, Y., Kimball, J. S., Jones, L. A., Reichle, R. H., & McDonald, K. C. (2011). Evaluation of MERRA land surface estimates in preparation for the soil moisture active passive mission. *Journal of Climate*, *24*, 3797–3816.

Yilmaz, M. T., & Crow, W. T. (2012). The optimality of potential rescaling approaches in land data assimilation. *Journal of Hydrometeorology*, *14*, 650–660.